ICES Journal of Marine Science, 2023, **80**, 197–209
DOI: 10.1093/icesjms/fsac226
Advance access publication date: 29 December 2022
Original Article

Correction of beam overlap-induced athwart distortion in multibeam sonars

Guillermo Boyra[1,*], Udane Martínez[1], Jon Uranga[1], Gala Moreno[2] and Héctor Peña[3]

[1]AZTI, Sustainable Fisheries Management, Herrera Kaia, Portualdea z/g, 20110 Pasaia (Gipuzkoa), Spain
[2]International Seafood Sustainability Foundation (ISSF), Suite #316, 3706 Butler Street, Pittsburg, PA 15201, USA
[3]Ecosystem Acoustics, Institute of Marine Research, N-5817 Bergen, Nordnes, Norway

[*] *Corresponding author: tel: +34 667 174 436; fax +34 946 574 000;* e-mail: gboyra@azti.es.

A method is proposed to estimate and correct athwart-beam distortion of multibeam sonars to advance sonar-based abundance estimation. We illustrate its application using data from a Simrad SN90 multibeam sonar aboard a tropical tuna purse-seiner, targeting mixed fish aggregations around drifting Fish Aggregating Devices (dFADs) in the Atlantic Ocean. To calculate the distortion in the horizontal swath, athwart-beam measurements were compared with the more accurate simultaneous along-beam measurements. For the vertical swath correction, we used as reference a vertically oriented single, split beam echosounder simultaneously monitoring the same aggregations. Along-to-athwart ratios of ∼0.6 and ∼0.3 were estimated for the horizontal and vertical swaths, respectively, at ranges involved during purse-seine operations in this fleet (from ∼225 to ∼325 m). Additionally, equations were developed to analytically describe the athwart distortion due to overlap between contiguous beams. Once corrected for distortion, typical school morphology measures were provided for tuna aggregations around dFADs.

Keywords: dFAD, purse-seiner, tropical tuna.

Introduction

Purse-seiners targeting tropical tuna extensively use drifting Fish Aggregating Devices (dFADs; Castro *et al.*, 2002) to aggregate and catch tuna. The skippers of these fishing vessels use sophisticated acoustic sensors, including echosounders and multibeam sonars, to detect and monitor fish aggregations (Moreno *et al.*, 2019). Long-range multibeam sonars are typically used to search for fish schools, whereas medium- to short-range models aid in the purse-seine maneuver and help making rough estimates of fish abundance found both in free-swimming schools and associated with dFADs (Gerlotto *et al.*, 2004; Korneliussen *et al.*, 2009).

Achieving accurate quantitative sonar-based estimations of fish aggregation volume and abundance could be helpful in both commercial and scientific scopes. In commercial fisheries, quantitative sonar measurements might increase the efficacy of fishing operations, and help to discriminate between the detected fish species before the net is set, hence reducing fish mortality by release of unwanted catches (or "slipping"; Marçalo *et al.*, 2019) and allowing for more selective fishing (Moreno *et al.*, 2019). In scientific research, quantitative multibeam sonars could provide avoidance measurements of close-to-surface species, improve target strength (TS) measurements using the comparison method (Misund and Beltestad, 1996), and achieve enhanced fishery-independent stock abundance estimations (Uranga *et al.*, 2019) based on sonar mapping (Hewitt *et al.*, 1976).

Traditionally, sonars have been analogue acoustic equipment that had to be analysed by applying image analysis on screen captures (Misund, 1993; Uranga *et al.*, 2017). However, the last generations of multibeam sonars record digital data (e.g. Trygonis *et al.*, 2009), adhere to standard acoustic data formats (Macaulay and Peña, 2018), and can be calibrated (Vatnehol *et al.*, 2015). In addition, one of their main advantages is their potential to provide three-dimensional size measurements of the targets they detect, thanks to the combined information from multiple beams.

However, it is still difficult to take advantage of the vast amount of acoustic data provided by multibeam sonars to obtain quantitative abundance estimates. Until recently, there was a general lack of information regarding the acoustic properties (i.e. target strength and frequency response) of tuna species surrounding dFADs. This made it difficult to interpret the collected information beyond the basics, although important research efforts have been made to obtain fundamental information on the acoustic properties of the main tropical tuna species over the past few years (Boyra *et al.*, 2018, 2019; Moreno *et al.*, 2019). Moreover, to make this acoustic tool useful for scientific purposes, other challenges must be addressed, owing to the nature and characteristics of these types of acoustic equipment.

Vertically oriented mono-beam echosounders are widely used to estimate the acoustic abundance of fish species (e.g. Doray *et al.*, 2021) or other ecosystem organisms (Korneliussen *et al.*, 2016). However, several difficulties arise when working quantitatively with multibeam sonars compared to echosounders. The acoustic backscattering energy recorded by multibeam lateral sonars is expected to be more variable than that of echosounders for various reasons: (1) being oriented laterally rather than vertically, the variability of the measured backscattering is expected to be greater owing to greater variability of the swimbladder cross-section with the fish yaw angle than with the fish tilt angle (Holmin *et al.*, 2011); (2) the non-vertical direction of the sonar beams can cause additional

Received: September 13, 2022. **Revised:** November 1, 2022. **Accepted:** November 28, 2022

variability in the obtained backscattering energy due to potential unknown curvature in the sound paths that might vary the amount of energy incident to the target (e.g. Medwin and Clay, 1998); and (3) the cross-talk between different beams distort the measured backscattering values, thus increasing the variability in the averaged acoustic energy (Vatnehol *et al.*, 2017).

Finally, and here resides the focus of this work, there are also difficulties in taking advantage of the potential benefits offered by sonars to estimate target dimension measurements using their multiple beams. Along-beam measurements obtained by sonars are known to be accurate to the order of tens of centimeters (or even a few centimeters) depending on the pulse length in narrowband (Simmonds and MacLennan, 2005) or the bandwidth in wideband acoustics (Demer *et al.*, 2017); however, athwart-beam measurements are more imprecise, with uncertainty increasing with the distance to the transducer due to geometric expansion of the beams (Misund, 1993; Diner, 2001). Furthermore, in an experiment conducted through simulation of a multibeam sonar (Vatnehol *et al.*, 2017), the athwart-beam measurements largely exceeded the distortion by geometric expansion described by Misund's equations, due to overlap between contiguous beams. Simulation-based empirical corrections were provided to remove athwart distortion caused by geometric expansion of the beams, which were proved accurate only at short ranges. In another study, Trygonis and Kapelonis (2018) corrected the size measurements of a Simrad SP90 multibeam sonar based on a simulation of individual beam patterns, accounting for the overlap between contiguous beams. However, their approach requires complex computations to simulate the emitted swath depending on the particular physical characteristics of the transducer, which might vary for different sonar systems. Therefore, for the time being, a general approach that provides a simple distortion correction for different models of multibeam sonar at different ranges is still missing.

One of the acoustic systems most commonly used by the industrial tropical tuna purse-seine fleet in recent years is the Simrad SN90 multibeam sonar (Kongsberg, 2020). The SN90 is a directional multibeam sonar with a medium–high frequency, operating in the frequency band from 70 to 120 kHz, in both narrow- and wide-band acoustic modes. On purse-seiners, it is usually installed on the hull, pointing laterally to the side. The flat transducer of this equipment, unlike those of omnidirectional sonars, does not need to be extended under the boat, allowing its use during the entire purse-seine maneuver with low risk of net entanglement. In addition, the SN90 has three split beam inspection beams, which provide additional scientific echosounder-like functionalities. This allows obtaining (at least in theory and within the possibilities of the available bandwidth) school abundance, *TS* analysis and frequency response of detected targets. That is, it provides simultaneous scientific echosounder functionality (i.e. identification of fish species and size, school density), and multibeam sonar functionality (i.e. estimation of aggregation size and shape, school density). However, no scientific study has evaluated the capabilities and limitations of this sonar equipment.

The objective of this study is to evaluate and improve the capabilities of multibeam sonars, particularly SN90, to estimate school dimensions. Acoustic data were registered on a tropical tuna purse-seiner during its regular commercial fishing activity around dFADs in the Atlantic Ocean to analyse the athwart distortion experienced in both the horizontal and the vertical swaths. Mixed tuna aggregations around dFADs were used as reference targets for the comparison. Then, following the earlier work by Misund (1993) as a starting point, as well as the recent developments by Vatnehol *et al.* (2017), equations were developed to explain the observed distortion, accounting for the percentage of overlap between contiguous beams. After correcting for distortion, the typical morphology of tuna aggregations around dFADs in this area were studied.

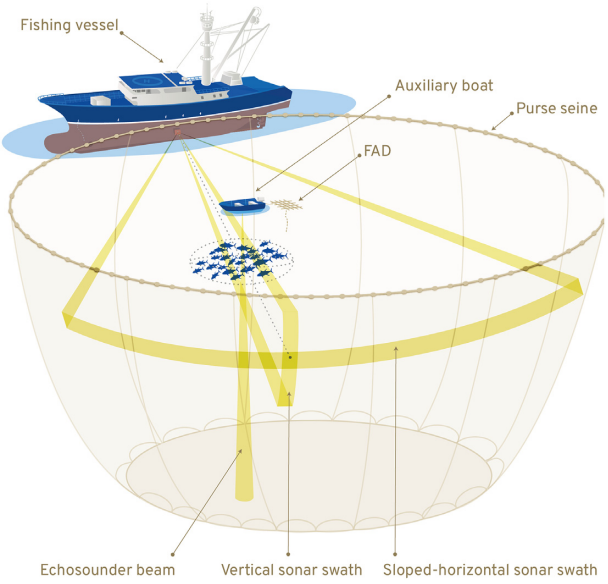

Figure 1. Illustration of the experimental setup, showing a schematic of the purse-seine maneuver as well as the diagram of the beams emitted by a Simrad SN90 multibeam sonar, distinguishing the horizontal and vertical swaths.

Material and methods

General description of the methodology

In purse-seining maneuvers, multibeam sonars are the main acoustic tools used by fishers to locate the targets and achieve a successful catch. During the encircling maneuver, the purse-seiner surrounds the aggregation building a cylindrical cage by releasing a rectangular net with floats on the top line and weights on the bottom (Figure 1). When the encirclement is complete, the bottom of the cylinder is closed, forming a basket to enclose the aggregation. Meanwhile, a smaller auxiliary boat is used to hold the dFAD during the aggregation encirclement. The vessel tightens the siege until the purse is sufficiently small to extract the fish from the boat using large brailers or suction pumps.

Two types of acoustic sensors were used in this study: the SN90 sonar of the tuna vessel itself, which monitored the aggregation laterally, and an EK80 scientific echosounder installed on the auxiliary boat, which monitored the aggregation vertically while it was surrounded by the net. The SN90 transmits two swaths simultaneously, one vertically oriented and the other horizontally oriented but sloped downwards (Figure 1). With these swaths, the SN90 provided concurrent measurements of the horizontal and vertical extents of aggregations. In order to measure the athwart-beam distortion, the mixed tuna aggregations found around the dFADs were used as reference targets. A basic assumption made for this analysis was that the size measurements made along the beam are generally free of distortion, and hence, were considered accurate.

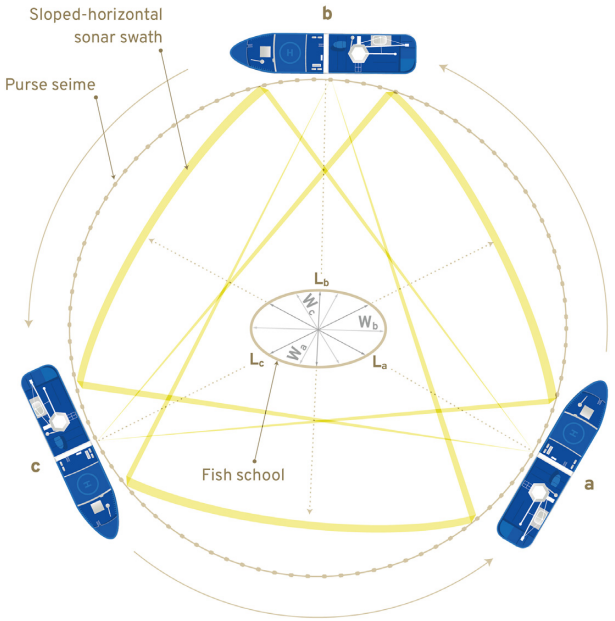

Figure 2. Top view of the purse-seine maneuver around a school of tuna to illustrate the method used to measure athwart distortion in the horizontal swath. The vessel is shown emitting a sonar swath at three successive positions during purse-seine deployment. At each instant, the sonar provides measurements of the diameter of the school in two directions: along beam (L) and athwart beam (W).

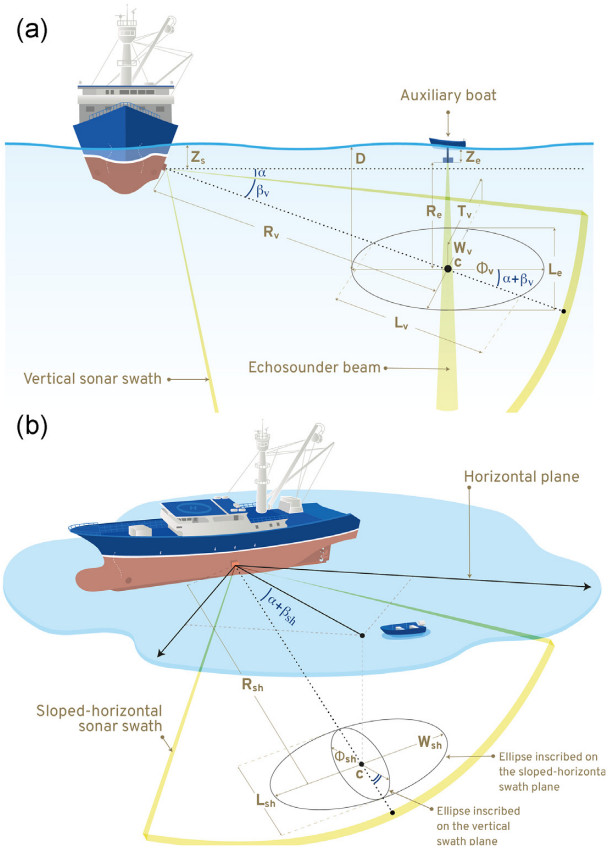

Figure 3. Geometric representation of the morphometric measurements performed by both acoustic sensors, the echosounder (marked with subindex "e") and the vertical (marked with subindex "v") and sloped-horizontal (marked with subindex "sh") swaths of the sonar, as well as the projected "true" school dimensions. (a) Vertical sonar swath vs. echosounder measurements. (b) Sloped-horizontal sonar swath measurements.

Two variants of the method were applied, one for each sonar swath.

In the case of the sloped-horizontal swath, taking advantage of the radial symmetry characteristic of the purse-seining maneuver, in which the sonar laterally monitors the aggregation from all directions while surrounding it in a circular trajectory, it was assumed that the along-beam (L) and athwart-beam (W) measurements from each fishing operation should be on average equal. Thus, we compared the average sloped-horizontal diameter measurements obtained along-beam and athwart-beam in each set (Figure 2). If the measurements were on average of the same size, it would mean that both measurements would be correct. However, if the athwart-beam measurements were larger than the along-beam ones (as expected), the latter would be considered the correct ones and would be used to correct the former.

To measure the athwart-beam distortion in the vertical swath of the sonar, the same technique could not be applied, because, in this swath, the along-beam and athwart-beam extents of the school are different measurements (horizontal diameter and height, respectively). Therefore, we resorted to another method, consisting in comparing the aggregation height measurements obtained with the sonar (W_v) and the vertical echosounder installed on the auxiliary vessel (L_e; Figure 3). Since the latter measurements are obtained along the beam, it was assumed that they were also correct and were used to adjust the height of the shoal measured by the vertical sonar swath.

Equipment

The data were collected during a commercial fishery campaign aboard the Curaçao-flagged tuna freezer vessel F/V Pacific Star, a 107-m-long purse-seiner with 4164 GT (2400 tonnes capacity). The survey ran from 27 November 2018 to 1 January 2019, starting and ending in Abidjan (Côte d'Ivoire), with a duration of 36 days. A total of 66 fishing operations were performed on the dFADs during the campaign, of which 44 provided simultaneous measurements of SN90 and EK80 (Supplementary Table SI-1). The purse-seine net used for fishing had a perimeter of ~1600 m and a height of 240 m, hence comprising a seining diameter of near 500 m, with a minimum mesh size of 15 cm in the central part. A random sample of at least 1% of the catch in each set was sized and sorted by species.

The Simrad SN90 multibeam sonar operated with a sloped-horizontal swath of 120° distributed in 32 beams and a vertical swath of 80° with 32 beams (Figure 4). The angular separation between contiguous beams was 3.75° in the sloped-horizontal swath and 2.5° in the vertical. According to the manufacturer's specifications, the receiver width of each individual beam is 6° at 100 kHz on centre axis, widening with increasing tilt and bearing angles (following the cosine of the angle) as well as with lower frequency. This would yield a minimum nominal percentage of overlap of 6°/3.75° = 1.6 (~60%). The vertical echosounder was a split-beam Simrad EK80 of 120 kHz, nominal beam width of 7° and a pulse duration of 512 μs.

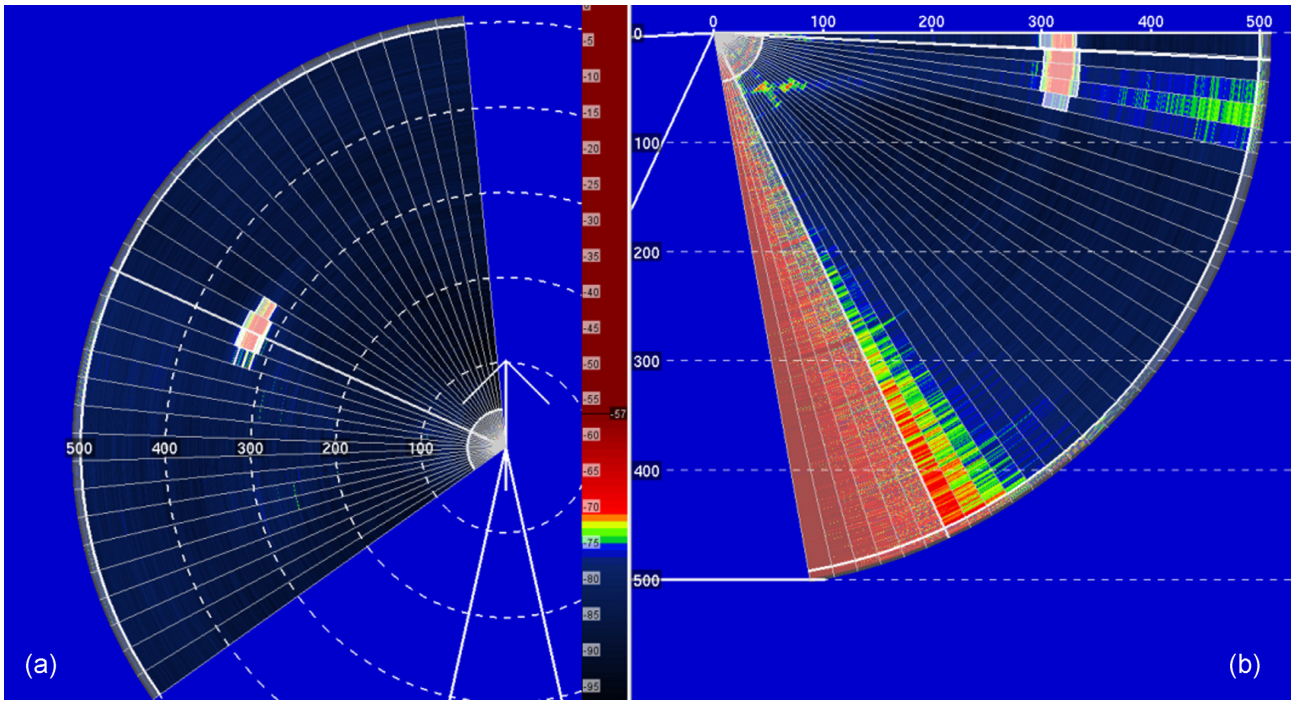

Figure 4. Screenshots of the LSSS-PROFOS software showing the individual beam composition of the sloped-horizontal (a) and vertical (b) swaths of SN90 in the configuration used in this study. Examples of fish schools are also included in both swaths, which are surrounded by a white outline by the software, to indicate that they have been identified as schools.

SN90 sonar recordings were made from the tuna vessel itself, with simultaneous EK80 echosounder data recordings obtained from the auxiliary boat (Figures 1 and 3). Sonar data processing was performed using the PROFOS module (Processing system for Omnidirectional Fisheries Sonar; Peña *et al.*, 2021) of LSSS software (Large Scale Survey System; Korneliussen *et al.*, 2016). Echosounder data processing was performed using Echoview Software Pty Ltd, 2013, version 5.2.

Data analysis

Temporal evolution of school dimensions

The morphometric parameters of the tuna aggregations were estimated using the SN90 multibeam sonar of the tuna vessel. Plots were constructed to visualize the temporal evolution of the pairs of along-beam and athwart diameters provided by the sloped-horizontal and vertical sonar swaths. These temporal evolution plots were used to evaluate (1) possible trends over the duration of the purse-seine maneuver and (2) whether a larger apparent size is appreciated in the athwart measurements, which would indicate distortion.

Correction of along beam dimensions

In both echosounders and multibeam sonars, the dimensions measured along the beam require subtraction of the length of the emitted pulse to provide unbiased measurements of the distance to the target

$$R = \frac{c\,(\Delta t\ -\ \tau)}{2}\ , \tag{1}$$

where c is the speed of sound (in m s^{-1}), Δt is the time elapsed from the emission of the acoustic pulse to its reception, and τ is the pulse duration (both in seconds). To measure the extent of a target along the beam, we applied the following equation:

$$L\ =\ R_{max}\ -\ R_{min}, \tag{2}$$

where R_{max} and R_{min} are maximum and minimum target ranges, respectively. In the case of the sonar, the along-beam extents of the aggregation measured were then used to estimate its horizontal diameter Φ. To estimate the horizontal school diameter measured by the vertical sonar swath, Φ_v, we projected L_v onto the horizontal plane (Figure 3a and Table 1). The sonar transducer was installed inclined at an angle α with the horizontal plane to avoid reverberations from waves at the sea surface. In addition, the beam targeting the centre of the aggregation was further tilted at an additional angle β_v, which we estimated from the sonar vertical echogram, as follows:

$$\beta_v = \mathrm{arcsin}\left(\frac{T_v}{R_v}\right), \tag{3}$$

where T_v and R_v are the distances from the centre of the aggregation to the top of the echogram and the sonar transducer, respectively (Figure 3).

To account for α and β_v in the estimation of the horizontal diameter, we assumed that the aggregations were ellipsoidal and oriented in parallel to the sea surface (Figure 3). Therefore, we applied the following transformation to convert the measured tilted diameter (L_v) into the horizontal diameter of the ellipse (Φ_v):

$$\Phi_v = \frac{L_v}{\sqrt{[\cos\,(\alpha+\beta_v)]^2 + \left[\frac{\sin(\alpha+\beta_v)}{\varepsilon_v}\right]^2}}. \tag{4}$$

Here, ε_v represents the mean elongation (i.e. the mean length-to-height ratio) of the near-ellipsoidal aggregations inscribed on the vertical swath plane, through the fishing operations,

Table 1. Dimensional measurements of the targets as read in each sensor's coordinate system and as projected to a common external one.

Measurement	Symbol	Coordinate system	Echosounder	Sloped-horizontal sonar swath	Vertical sonar swath
Range	R	Sensor	R_e	R_{sh}	R_v
Along-beam size	L	Sensor	L_e	L_{sh}	L_v
Athwart-beam size	W	Sensor	-	W_{sh}	W_v
Depth	D	Common	D_e	D_{sh}	D_v
Height	H	Common	H_e	H_{sh}	H_v
Diameter	Φ	Common	Φ_e	Φ_{sh_L}, Φ_{sh_W}	Φ_{v_L}, Φ_{v_W}

calculated as follows:

$$\varepsilon_v = \frac{\Phi_v}{L_e}, \tag{5}$$

where L_e is the height of the aggregation, measured using the vertical echosounder.

A circular bond exists between Equations (4) and (5), because obtaining the horizontal diameter of the aggregation (Φ_v) from the along-beam measurement of the sonar (L_v) requires knowing the elongation of the aggregation, which in turn depends on the horizontal diameter. Both equations were solved recursively to break the circularity. The procedure was as follows: we applied an initial value $\Phi_v = L_v$ to calculate the elongation using Equation (5) and then used this to calculate the horizontal diameter with Equation (4). If the obtained diameter differed from the initial diameter, it was used to obtain a new elongation value using Equation (5), and, with this elongation, another diameter using Equation (4). This process was repeated until convergence was achieved, that is, until the input and output diameters were equal.

The projection of the tilted aggregation extension measured by the sonar to the horizontal plane was done equivalently for the sloped-horizontal swath but is omitted here to avoid repetitions.

Correction of sloped-horizontal athwart distortion

Numerical correction based on the along-to-athwart beam ratio

Statistical comparisons were performed to evaluate the parameters provided by the acoustic sensors used in the tuna vessel. The pairs of along- and athwart-beam diameters provided by the sloped-horizontal swath of the sonar were compared to evaluate whether a greater apparent size was observed in the athwart measurements, which would indicate distortion. For each fishing operation (i) diameter measurements were taken along-beam and athwart-beam for all pings, and the average along-to-athwart fraction (F_{sh_i}) was calculated as follows:

$$F_{sh_i} = \frac{\Phi_{sh_{L\,i}}}{\Phi_{sh_{W\,i}}}, \tag{6}$$

where $\Phi_{sh_{L\,i}}$ and $\Phi_{sh_{W\,i}}$ are the average along- and athwart-beam horizontal diameters, respectively per set for all pings. Next, the average athwart correction fraction across all fishing operations, F_{sh}, was computed for the sloped-horizontal swath as follows:

$$F_{sh} = \frac{\sum_i F_{sh_i}}{N}. \tag{7}$$

Finally, a corrected athwart diameter was obtained for each ping of each fishing operation by multiplying the uncorrected diameter by the average along-to-athwart fraction

$$\Phi_{sh_{W,\,corr}} = F_{sh}\ \Phi_{sh_W}. \tag{8}$$

Analytical correction based on the percentage of overlap

As mentioned above, athwart distortion has been reported to increase with the distance to the target (Vatnehol *et al.*, 2017). It is, therefore, convenient to correct for distortion as a function of distance rather than simply statistically as a single overall ratio. Thus, once the athwart diameter corrections were obtained as ratios, they were interpreted analytically and projected as a function of the basic geometry of the beams of a multibeam sonar, as we explain below.

To measure the extent of a fish school in the athwart beam direction, the number of beams in which it appears (N_{sh}) is counted and multiplied by the width of a beam at a given distance (R_{sh}), as a function of the separation angle between contiguous beams (φ_{ang}) as follows:

$$\Phi_{sh_W} = 2N_{sh}R_{sh}\tan\left(\frac{\varphi_{ang}}{2}\right). \tag{9}$$

To correct for the bias caused by the increasing size of the beams, Misund (1993) applied a correction consisting of subtracting the width of an entire beam. This is indicated by subtracting 1 from N_{sh} in the following expression:

$$\Phi_{sh_{W,\,Misund}} = 2\,(N_{sh} - 1)\,R_{sh}\tan\left(\frac{\varphi_{ang}}{2}\right). \tag{10}$$

In this work, a variant of that correction was applied, consisting in the subtraction of only half of the individual beamwidth, so that the width of a target visible in one beam (N_{sh}= 1) does not result in a measurement of zero diameter, but in half of the beam diameter at that distance. The equation is transformed into the following:

$$\Phi_{sh_{W,\,Misund2}} = 2\left(N_{sh} - \frac{1}{2}\right)R_{sh}\tan\left(\frac{\varphi_{ang}}{2}\right). \tag{11}$$

An additional correction term was added to the athwart dimension calculation to account for the distortion introduced by the percentage of overlap, PO_{sh}, between adjacent beams as follows:

$$\Phi_{sh_{W,\,corr}} = 2\left(N_{sh} - PO_{sh} - \frac{1}{2}\right)R_{sh}\tan\left(\frac{\varphi_{ang}}{2}\right). \tag{12}$$

The percentage of overlap is defined as the excess width of the individual beams (φ_{bw}) with respect to the angular distance between adjacent beams (φ_{ang}), measured as a proportion of φ_{ang} as follows:

$$PO_{sh} = \frac{\varphi_{bw} - \varphi_{ang}}{\varphi_{ang}} = \frac{\varphi_{bw}}{\varphi_{ang}} - 1. \tag{13}$$

Notice that PO_{sh} is positive when $\varphi_{bw} > \varphi_{ang}$, zero when $\varphi_{bw} = \varphi_{ang}$, and can be forced to zero also for $\varphi_{bw} < \varphi_{ang}$ (because a correction would not be necessary in this case). If $\varphi_{bw} = \varphi_{ang}$, the percentage of overlap is zero, and Equation (12) simplifies into Equation (11).

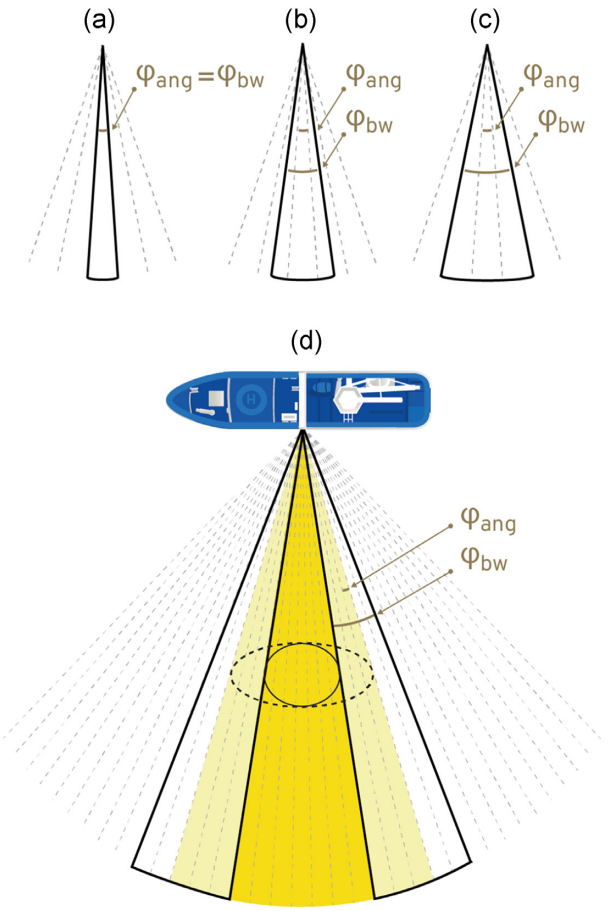

Figure 5. Illustration of the mechanism producing overlap-based athwart distortion in multibeam sonars described by Equations (12) and (14) in the horizontal swath (equivalent to that described by Equations (19) and (20) in the vertical swath). We highlight the difference between the angular distance between adjacent beams, φ_{ang}, and the width of the individual beams, φ_{bw}. In (a) there is no overlap between beams, $\frac{\varphi_{bw}}{\varphi_{ang}} = 1$, and the percentage of overlap, PO_{sh}, is zero. However, as φ_{bw} surpasses φ_{ang}, overlapping between adjacent beams occurs. These are the cases shown in (b) where $\frac{\varphi_{bw}}{\varphi_{ang}} = 2$ and in (c) where $\frac{\varphi_{bw}}{\varphi_{ang}} = 3$. In (d), where $\frac{\varphi_{bw}}{\varphi_{ang}} = 5$, it is shown the distortion produced on the athwart dimension of a target as effect of overlapping. In this idealized case, the first three beams outside the true edge of the target can detect the aggregation from each side, thus changing the apparent shape of the target from a circle (solid line) to a wider ellipse (dashed line).

As an alternative to Equation (12), we can express $\Phi_{sh_{W,\,corr}}$ as a function of $\frac{\varphi_{bw}}{\varphi_{ang}}$ instead of the percentage of overlap [by substituting Equation (13) into Equation (12)] and explicitly showing the dependence on the uncorrected diameter (Φ_{sh_W}) yielding

$$\Phi_{sh_{W,\,corr}} = \Phi_{sh_W} - 2\left(\frac{\varphi_{bw}}{\varphi_{ang}} + \frac{1}{2}\right) R_{sh} \tan\left(\frac{\varphi_{ang}}{2}\right). \quad (14)$$

The interpretation of this new term in Equations (12) and (14) is as follows: in order to correct the athwart size measured by a multibeam sonar, we subtract from the apparent size seen in the echogram the contribution of those first peripheral beams near the edge of the aggregation that, due to beam overlapping, are able to detect it (Figure 5).

To obtain an effective beam width value (φ_{bw}) for the SN90 horizontal sonar swath, an optimization procedure was conducted, adjusting the following equation obtained by linking Equations (8) and (14) as follows:

$$F_{sh}\ \Phi_{sh_W} = \Phi_{sh_W} - 2\left(\frac{\varphi_{bw}}{\varphi_{ang}} + \frac{1}{2}\right) R_{sh} \tan\left(\frac{\varphi_{ang}}{2}\right). \quad (15)$$

Equation (15) was computed for a sequence of φ_{bw} values (0°, 1°, …, 90°), and the angle that maximized the agreement between both sides for all fishing operations was chosen as the optimum.

Correction of vertical athwart distortion

Numerical correction based on the along-to-athwart beam ratio. To measure the athwart correction in the vertical swath, we compared the aggregation height measurements obtained with the sonar with those from the vertical echosounder installed on the auxiliary vessel (see Figures 1 and 3).

Echosounder data analysis consisted of several steps to automatically determine the representative height of each fish aggregation. First, a "school processing," that is, a segmentation process to obtain regions delimiting the aggregation (Reid, 2000), was applied to the echograms, using the default parameters in Echoview school processing tool plus a −60 dB minimm threshold, frequently used in acoustic echointegration-based fish abundance estimates to distinguish between fish and plankton (e.g. Doray *et al.*, 2021). Afterwards, these regions were transformed into bitmaps and used to mask shoals on the echogram, deleting anything apart from schools. The masked echograms were then divided into cells of one ping per one meter height. The 1-m length heights of the cells retained by the mask were summed, thus cumulatively producing the total height of the shoal for each ping (Supplementary Figure SI-1).

However, because the auxiliary boat had limited mobility, sampling exactly the centre of the school was not ensured, which might have caused the echosounder to underestimate the height of the aggregation. To prevent underestimation of heights, rather than directly applying the mean or median as their most representative central estimator, a percentile was chosen with a probability obtained by optimization. Thus, the percentile of the school height for a sequence of probabilities from 1 to 100% was calculated, and linear regressions were fitted between the school height percentile for the different probabilities and the catch of the fishing operations of the campaign. The percentile, $R_{e,\,cor}$, whose probability maximized the coefficient of determination of the regressions, was chosen as the optimum.

On the other hand, to compare the measurements made by the two different sensors (sonar and echosounder) the installation depth of both had to be considered as well as the tilt angle of the sonar transducer, and the orientation of the beams targeting the centre of the aggregation (Figure 3). Thus, because the absolute depth of the aggregation should be the same in both sensors, the following equation was used to relate the measurements of each sensor:

$$D = z_s + R_v \sin(\alpha + \beta_v) = z_e + R_{e,\,cor}, \quad (16)$$

where $\alpha = 6°$ is the installation tilt angle of the sonar transducer on the hull, β_v is the inclination angle of the sonar beam targeting the centre of the aggregation, $z_s = 6$ m is the depth of the sonar transducer, and $z_e = 1$ m is the depth of the echosounder. The inclination angle, β_v, was obtained from the vertical sonar measurements using Equation (3).

In addition, given the installation and operative tilt angles used, at the typical horizontal distance of ∼275 m from the aggregations, the upper part of the vertical swath was at a

depth of 35 m, hence missing the upper part of the aggregations in many cases. In order to avoid measurements of partial aggregations, in the vertical swath analysis, those purse-seine operations in which the minimum depth of the aggregation was above the upper limit of the vertical swath were filtered. In the remaining cases, the mean distortion correction factor was calculated as the average along-to-athwart fraction across the sets as follows:

$$F_v = \frac{L_e}{H_v} = \frac{L_e}{W_v\sqrt{[\cos(\alpha+\beta_v)]^2 + \left[\frac{\sin(\alpha+\beta_v)}{\varepsilon_v}\right]^2}}, \quad (17)$$

where ε_v is obtained from Equation (5). The vertical swath along-to-athwart fraction, F_v, was then applied as a factor to correct the vertical swath athwart dimension measurements, W_v, that is

$$W_{v,\,corr} = F_v\, W_v. \quad (18)$$

Analytical correction based on the percentage of overlap

Similar to the horizontal swath, once the numerical correction was obtained, it was interpreted as a function of the percentage of overlap of the vertical swath (PO_v) defined as a function of the ratio between the width of an individual vertical beam and the distance between contiguous vertical beams, $\frac{\theta_{bw}}{\theta_{ang}}$. The used equations were similar to those of the horizontal case (see the sloped-horizontal swath section for details):

$$H_{v_{W,\,corr}} = H_v - 2\left(\frac{\theta_{bw}}{\theta_{ang}} + \frac{1}{2}\right) R_v \tan\left(\frac{\theta_{ang}}{2}\right), \quad (19)$$

or, equivalently

$$H_{v_{W,\,corr}} = H_v - 2\left(PO_v - \frac{1}{2}\right) R_v \tan\left(\frac{\theta_{ang}}{2}\right). \quad (20)$$

The widths of the individual beams of the vertical swath were obtained by optimizing an equation equivalent to Equation (15) as follows:

$$F_v\, H_v = H_v - 2\left(\frac{\theta_{bw}}{\theta_{ang}} + \frac{1}{2}\right) R_v \tan\left(\frac{\theta_{ang}}{2}\right). \quad (21)$$

Study of tuna aggregation morphology in dFADs

Once the athwart measurements were corrected, we studied the school dimensions observed in the different fishing operations during the campaign. Specifically, the horizontal and vertical diameters to estimate the typical elongations in both directions were studied. We also analysed the relationship between aggregation dimensions as a function of catch.

Results

Temporal evolution of school dimensions

Figure 6 shows the relative positions of the fishing vessel, the tuna aggregation, and the auxiliary boat during the circling maneuver thorough the fishing operations. The typical deployment of the net took ~5 min (300 s), tracing near circular-shaped trajectories with diameters of ~500 m, so that the aggregations were at a typical distance of between 225–325 m from the tuna vessel during the maneuver. The auxiliary boat moved slowly inside the purse-seine, trying to stay away from the net. It usually stood on top of the aggregation, but in a slightly lopsided manner, so that on some occasions, the vertical sounder sampled the periphery rather than the centre of the aggregation.

As for the temporal evolution of the parameters measured by the sonar, the sloped-horizontal diameters showed two important aspects (Figure 7a): first, the athwart diameter was consistently larger than the along-beam diameter, thus confirming the existence of overestimation in the athwart direction; second, the temporal evolution showed no tendency of any of the aggregation diameters to decrease during the set, suggesting that, at least in the first minutes of the maneuver, and before the closure of the purse-seine, the aggregation dimensions remained relatively constant and presumably similar to those that the aggregation had before the arrival of the tuna vessel. In the measurements made on the vertical sonar swath (Figure 7b), the temporal evolution did not exhibit a clear tendency to decrease or increase during the set.

The temporal evolution of the minimum and maximum aggregation depths measured by the echosounder installed on the auxiliary boat shows that both these and the vertical height of the aggregation evolved throughout the set, but did not show tendencies of increasing or decreasing their vertical extent until the moment of seine closure (Supplementary Figure SI-2). Aggregation heights ranged between 10 and 20 m. In 12 out of 33 operations, the tuna aggregation was not entirely visible in the vertical swath of the sonar.

Correction of sonar athwart distortion

Horizontal swath

The difference between along-beam and athwart diameters showed a general distortion when measuring sizes in the athwart direction that tended to overestimate the diameters by ~80% (Figure 8, Table 2). The application of the numerical correction (consisting of multiplying by 0.58) was shown to correct the distortion providing unbiased measurements.

However, the athwart distortion increased with the distance to the target (Figure 9a). Thus, the numerical correction was able to correct the distortion on average, but not to eliminate the tendency of the distortion to grow with range. The analytical, overlap-based distortion correction obtained using Equation (12) did achieve both (Figure 9a).

The use of analytical distortion correction using Equation (12) yielded a percentage of overlap between beams of 2.5, that is, given a distance between contiguous beams of 3.75°, the effective aperture of the individual beams would be ~13° (Table 2).

Vertical swath

In the quartile optimization performed to summarize the shoal height measured by the echosounder, the quantile that maximized the correlation with the catches was found to be 0.5, which was very close to the mean value. Once the optimal quantile was applied, the difference between the vertical athwart diameter of the sonar and the along-beam diameter of the echosounder showed an overall athwart distortion that tended to overestimate the diameters by a factor of 3.5 (Figure 8). The application of the numerical correction (consisting of multiplying by 0.29) provided unbiased measurements.

The analytical correction for athwart distortion as a function of the percentage of overlap using Equation (17) provided

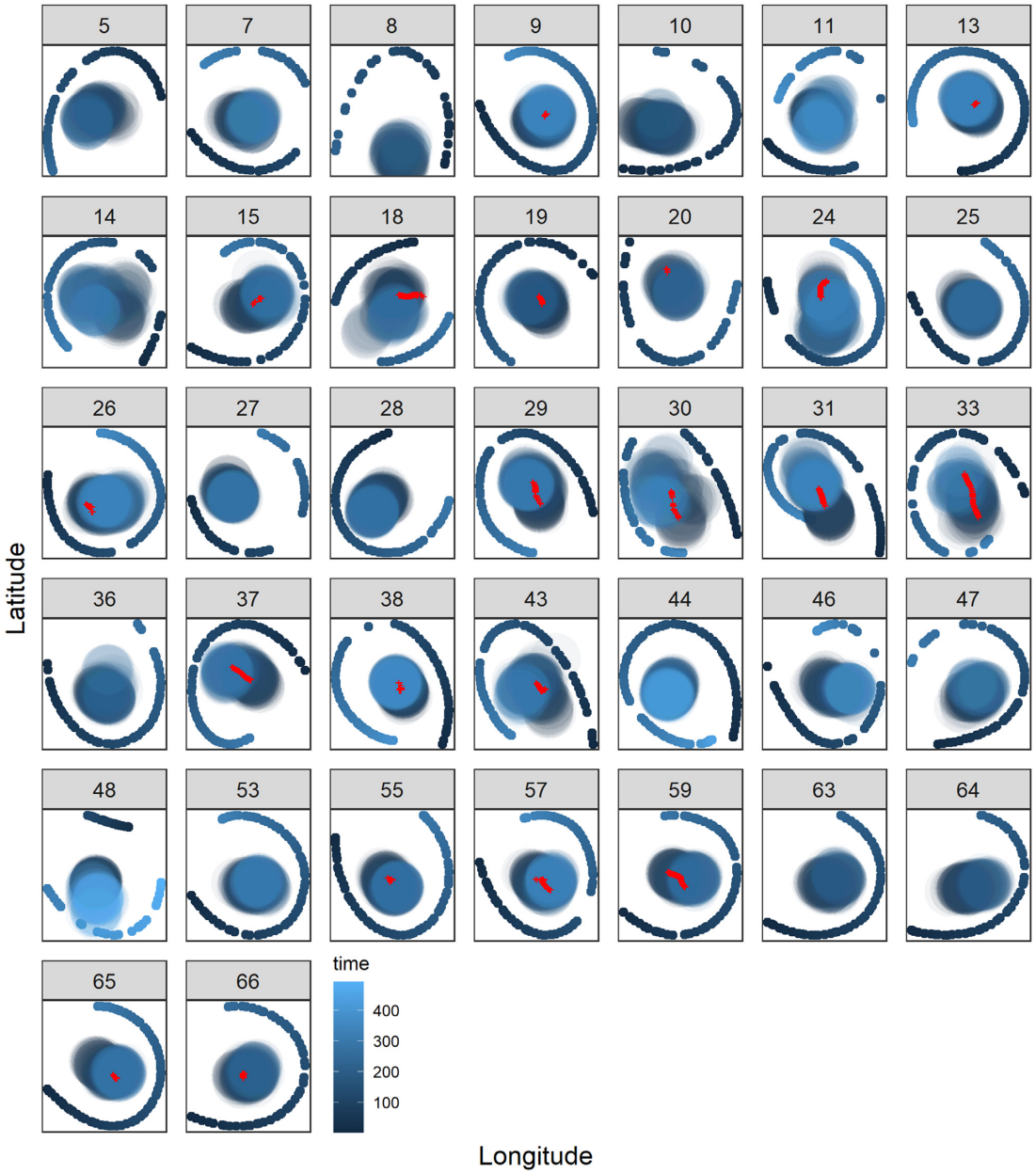

Figure 6. Top zenithal view of the acoustically monitored purse-seine maneuvers in the campaign. The dots show the position of the tuna vessel, and the fuzzy circles show the position of the aggregation during the maneuver (the colour indicates the time elapsed in seconds since the start). The small crosses (red online) show the position of the logistic vessel during the same period (when GPS data were available). The numbers on the top of each panel indicate the code of the corresponding fishing station. The extent of both axis of the figures is ~500 m in all panels.

an effective angle of 7°, which translates to a percentage of overlap of 1.8 (Table 2). However, in this case, the application of the analytical approach was not able to correct the increase of distortion with range (Figure 9b).

Morphology of tuna aggregations in dFADs

The typical diameter of schools in dFADs observed in this study was between 50 and 100 m approximately (Figure 10). This diameter increased linearly with catches ($p < 0.001$; Table 3), 50 m for catches on the order of 10 tonnes, and 100 m for catches of 90 tonnes. Mean aggregation heights were ~18 m. Height also grew linearly with catch ($p = 0.005$).

Tuna aggregations in dFADs tended to form elongated shapes horizontally; schools were four times as wide as they were tall, and this ratio did not appear to vary with catch (Figure 10). The average depth was between 45 and 50 m, and did not vary with catch.

Discussion

This study covers several related tasks with the goal of achieving and improving fish school size estimation using multibeam sonars. A methodological approach to measure and correct athwart distortion for multibeam sonars is described as part of the process to provide an abundance estimation. In addition, an equation to analytically explain and correct the ob-

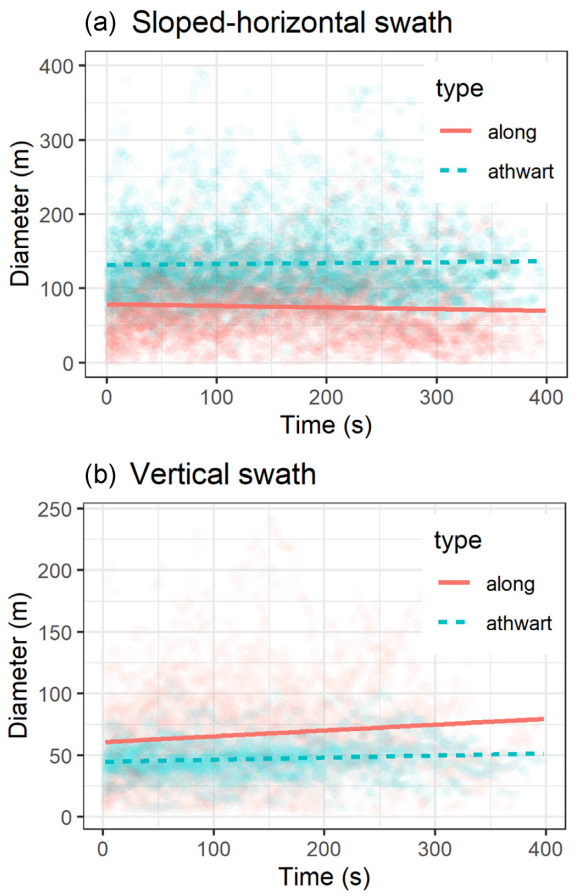

Figure 7. Mean temporal evolution of the aggregation extent measured by the horizontal sonar swath (a) and the vertical sonar swath (b) along and athwart the direction of the emitted beam throughout the purse-seine maneuvers carried out during the campaign. The straight lines represent linear regression models to highlight the tendencies. The dots are printed with certain degree of transparency to avoid overplotting; therefore, the colour intensity denotes density of measurements. Notice that, while in the horizontal sonar swath both measures refer to the same aggregation characteristic (its diameter), in the vertical swath, each corresponded to a different characteristic: the along-beam measurement was the aggregation diameter and the athwart-beam, its height.

tained distorted dimension values is presented. The method is demonstrated on a particular multibeam sonar model, the Simrad SN90, at typical operative target ranges for tuna fleet fishing around dFADs.

The correction methodology proposed was different for each swath of the sonar; for the horizontal athwart measurements, it was performed by comparison of along-beam measurements of the sonar itself, but the vertical swath required comparison with data from another concurrent acoustic equipment (a vertical echosounder; Figure 3). In an earlier study using multibeam sonars, Vatnehol *et al.* (2017) attempted distortion correction of another model of multibeam sonar, the SX90. There are several differences with the previous work. Apart from the sonar type, in their study, the analysis was based on model simulations. In addition, they corrected only for the geometrical spreading of the individual beams (not overlapping); thus, their result could only succeed in correcting the distortion at short ranges, when the overlapping effect is not too large, whereas in our case, the analytical correction accounting for the beam overlap is valid in principle for any target range, at least in the typical ranges involved when using multibeam sonars.

In another recent attempt to calibrate distortion (Peña *et al.*, 2021), large targets with known dimensions were used as references. The methodology presented here does not require the availability of a steady, large target of a known size (which can sometimes be impossible to obtain). Instead, it proposes the use of fish schools as a reference. However, owing to the changing nature of these targets, the availability of a relatively large number of fishing stations is required to be able to make a statistical comparison. Hence, our method is especially convenient when working in fishing vessels in commercial fishing activity, as we present here. Another difference between the two studies is that we obtained independent correction values for each swath, while they only obtained a single correction value for the horizontal swath.

The obtained numerical correction values are valid for this particular sonar model and configuration (120° horizontal and 80° vertical swath widths with 32 beams each, Figure 4 and Table 2) and typical range of distances to the target involved during purse-seine operations around dFADs, that is, from ∼225 to ∼325 m, given the perimeter of the net used (Figure 6). However, due to the way they were calculated, they cannot be extrapolated to different ranges. The configuration in the vertical cannot be changed; however the configuration in the horizontal can be set to higher swath widths (up to 160°) and different number of beams (16 or 64). A pending work is to repeat this study using the full range of apertures and beam numbers available to see changes in the observed distortions and the percentages of overlap involved are observed.

The developed analytical equations have the benefit of explaining the high distortion obtained by accounting for the percentage of overlap of the beams. This is a novel aspect of this work, as it extends the formulas developed by Misund (1993) to explain the athwart distortion in terms of the geometric expansion of the beams, adding an independent term that describes the overlap of the individual beams conforming each swath (Figure 5). Vatnehol *et al.* (2017) reported the limitations of Misund's formula in correcting the observed distortion, and proposed overlap as the cause of the extra amount of distortion. They pointed out the existence of a range of distances at which Misund's formula does not hold and noticed that this was related to the percentage of overlap as defined in this paper. However, they did not attempt to provide a correction for this distortion, limiting their goal to applying the correction only at short ranges. In our case, we have gone a step further, proposing an analytical correction for beam overlap that not only corrects the distortion at both ranges, but also explains it in geometrical terms that are simple to understand and calculate.

Trygonis and Kapelonis (2018) also proposed a method to correct distortion in multibeam sonar measurements for a different sonar model (Simrad SP90) and following a different approach. They relied on simulations of the directivity pattern of the individual beams of a multibeam sonar, whereas our work further simplified the consideration of each beam as its equivalent cone. Thus, the work of Trygonis and Kapelonis is more detailed, considering factors, such as secondary lobes and sonar extinction with range, that are ignored here. In return, our work provides a simplified equation for calculating the distortion correction from a parameter, the percentage of overlap, which must be measured experimentally. Interest-

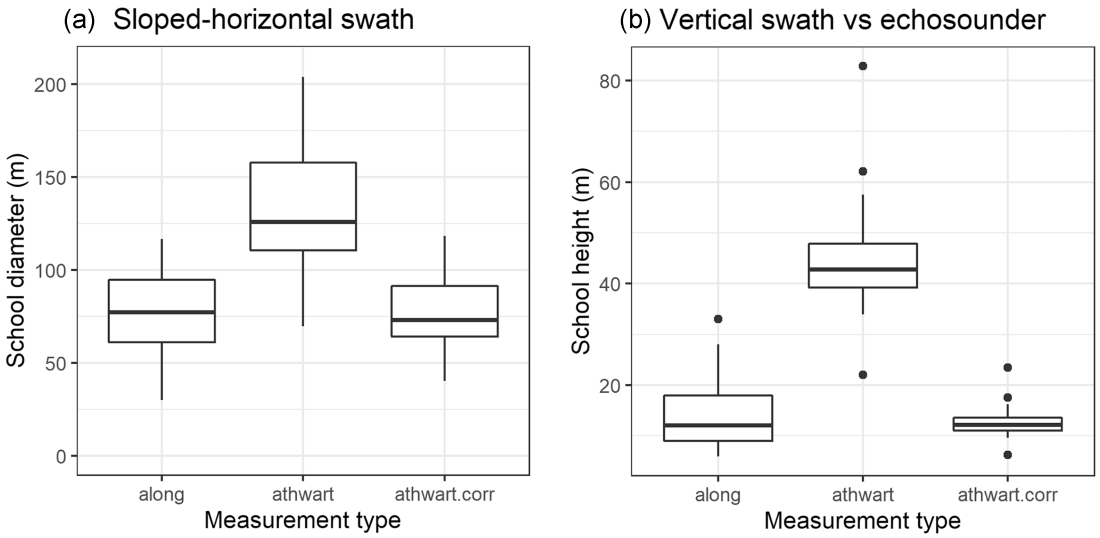

Figure 8. Boxplots showing the difference between along and athwart, with and without correction, on the measurement of the aggregation diameters for the horizontal swath (a) and heights for the vertical swath (b). In the vertical swath panel, the along-beam measurements are provided by the echosounder and athwart ones by the sonar. The dots represent outliers.

Table 2. Characteristics of both swaths of the Simrad SN90 sonar as used in this work, as well as the obtained distortion, effective beam width and overlap.

Sloped-horizontal swath		
Number of beams	N_o	32
Swath beam width (°)	φ_{swath}	120
Angular inter-beam separation (°)	φ_{ang}	120/32 = 3.75
Individual beam width (°)	φ_{bw}	13
Percentage of overlap	PO_{sh}	2.5
Along-to-athwart correction fraction	F_{sh}	0.58
Vertical swath		
Number of beams	N_v	32
Swath beam width (°)	θ_{swath}	80
Angular inter-beam separation (°)	θ_{ang}	80/32 = 2.5
Individual beam width (°)	θ_{bw}	7
Percentage of overlap	PO_v	1.8
Along-to-athwart correction fraction	F_v	0.29

ingly, despite the methodological differences between the two studies, the numerical corrections obtained in both cases for the sloped horizontal swath of each sonar model were of the same order (~0.6 in both cases), although it would be necessary to experimentally determine what the SP90 percentage of overlap is to be able to more rigorously compare both corrections. The percentage of overlap obtained here for the horizontal swath seems reliable, as it was able to correct not only the mean distortion obtained in the studied purse-seine operations, but also the tendency to increase the distortion with target range (Figure 9).

It must be noted, though, the inability of the analytical correction of the vertical swath to remove the increase in distortion with range, which prevented obtaining a reliable overlap index for the vertical swath with these data. There are several possible explanations for this. First, there was considerably less data to correct in the vertical than in the horizontal swath. For the vertical correction, there was only one measurement per set (rather than one per ping, as in the horizontal swath). Moreover, almost 2/3 of the sets were removed from the analysis of the vertical sonar swath because they did not cover the entire aggregation (Supplementary Figure SI-2). Second, there was higher uncertainty in both measurements of school height (sonar and echosounder) than in those of the horizontal school diameter. The need to connect the measurements of two sensors installed on different vessels (Figure 3) might have affected the calculations due to inaccuracies in the installation parameters of both sensors. Also, the lack of simultaneity between sonar and echosounder measurements due to synchronization issues, and the greater difficulty in targeting the centre of the aggregation for the auxiliary boat (which had to sail through the area encircled by the purse-seine) might have affected the accuracy of the vertical swath correction values. More experiments are required to obtain a more robust estimate of the percentage of overlap in the vertical swath.

The theoretical equations developed imply the existence of an effective beam aperture that is different from the angular separation between contiguous beams, which would cause overlap (Figure 5). The percentage of overlap estimated with this method was 2.5 for the horizontal swath, implying an effective beamwidth of ~13°, which is similar to that reported by Peña *et al.* (2021) for SX90 and SU90 multibeam sonars. The value obtained here was larger than the minimum horizontal beamwidth of 6° estimated by the manufacturer. It should be noted, though, that this effective beam width might not coincide with the theoretical overlap in the sensor specifications. This is because the definition and the method to calculate this effective beam width differs from the nominal beam width as it is normally calculated (i.e. as the width at which the gain of the directivity pattern of each beam falls to half the intensity of the maximum). Both magnitudes are probably related, but the magnitude included in Equations (12) and (17) depends on the difference between the acoustic backscattering of the target and the echointegration threshold applied,

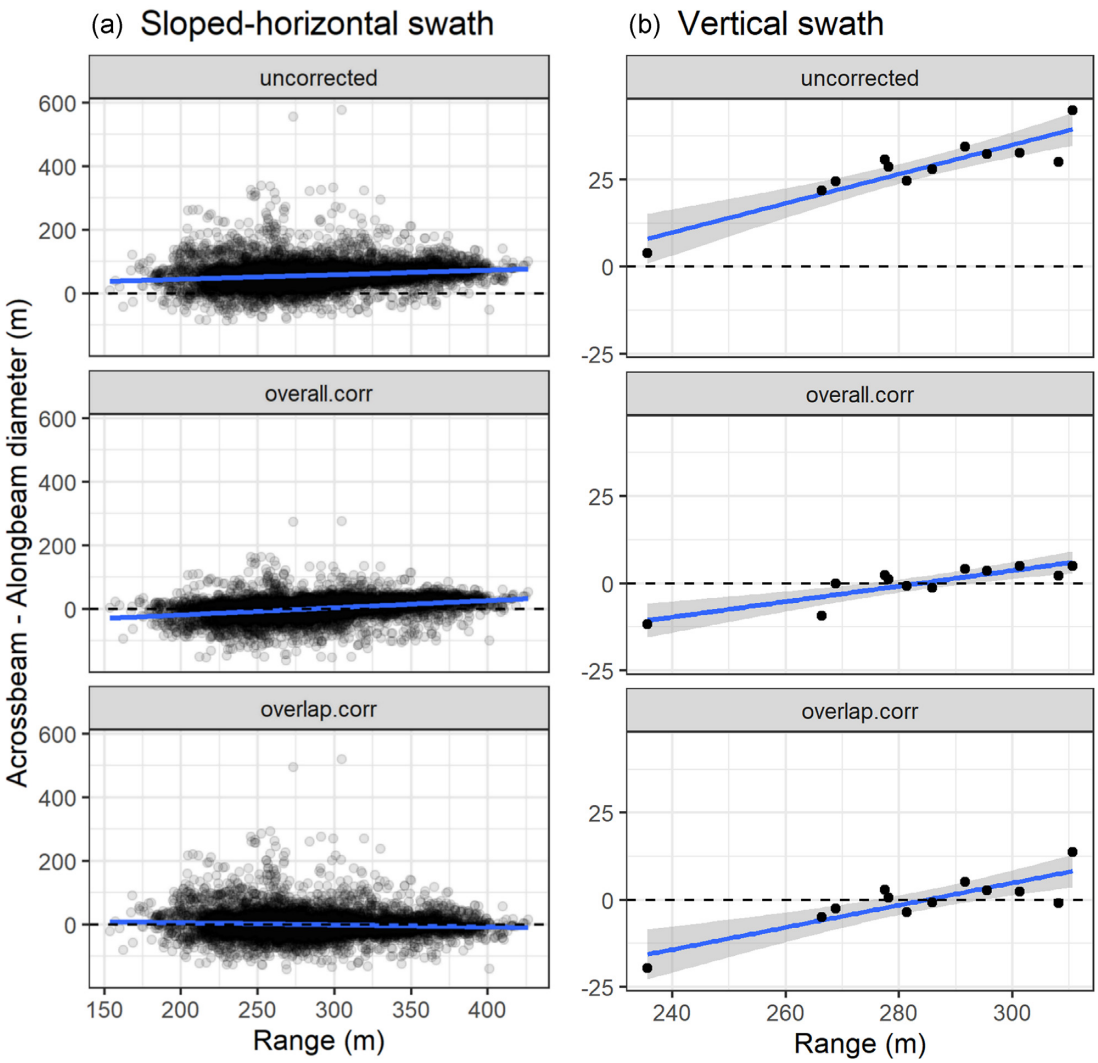

Figure 9. Scatterplots of athwart distortion vs. range (i.e. the distance from sonar transducer to the fish aggregation) before and after overall and overlap-based corrections. The blue line marks the trends by linear regression and, the grey shades, the confidence intervals. Notice that for the horizontal swath, each point represents a ping, while for the vertical swath each point represents the average across pings of a fishing operation.

whereas the nominal beam width does not. One could argue that it would be preferable to relate the distortion to an independent magnitude rather than one dependent on the echo strength of the target and the operative threshold applied, but the authors are afraid that according to their experience, unfortunately, the distortion, especially in the athwart direction, seems to be unavoidably dependent on the threshold and gain of the sonar, as well as the density of the observed target.

An additional outcome of this work is the corrected morphology of tuna aggregations in dFADs (Figure 10). These measurements of typical elongation and width of aggregations, in relation to the catch, could be potentially helpful in correcting the estimated biomass obtained by acoustic buoys placed in the dFADs (Lopez *et al.*, 2016; Moreno *et al.*, 2016; Orue *et al.*, 2019). So far, the abundance estimation provided by buoy echosounders uses the volume sampled by the acoustic beam as a proxy for the aggregation volume, because it lacks the horizontal aggregation parameter to calculate it. However, if a relationship exists between the aggregation diameter and a known variable (for example, the aggregation height), this dependency could be included in the calculations, potentially improving the estimation of the aggregation volume. The morphometric measurements obtained in this study are valid for a specific area of the Atlantic Ocean in a given year and within the catch range of the study (10–90 tonnes), which might be of anecdotal value yet. However, we believe that the acquisition of a more comprehensive set of morphometric measurements would be helpful to improve volume prediction from echosounder buoys. This set of parameters could include a wider range of school sizes, from a large number of dFAD casts to yield robust statistics of tuna aggregation characteristics, while also considering other oceanographic variables (e.g. mixing layer depth, upwelling index, or oxycline depth) to adjust and improve their predictions.

Once the athwart distortion is corrected for, SN90 multibeam sonars appear to be able to provide unbiased, reliable school sizes of tuna (and presumably other species). This was evidenced by the significant ($p < 0.01$), although relatively weak ($R^2 < 0.5$), correlations observed between measured aggregation sizes (i.e. horizontal diameter and height), and

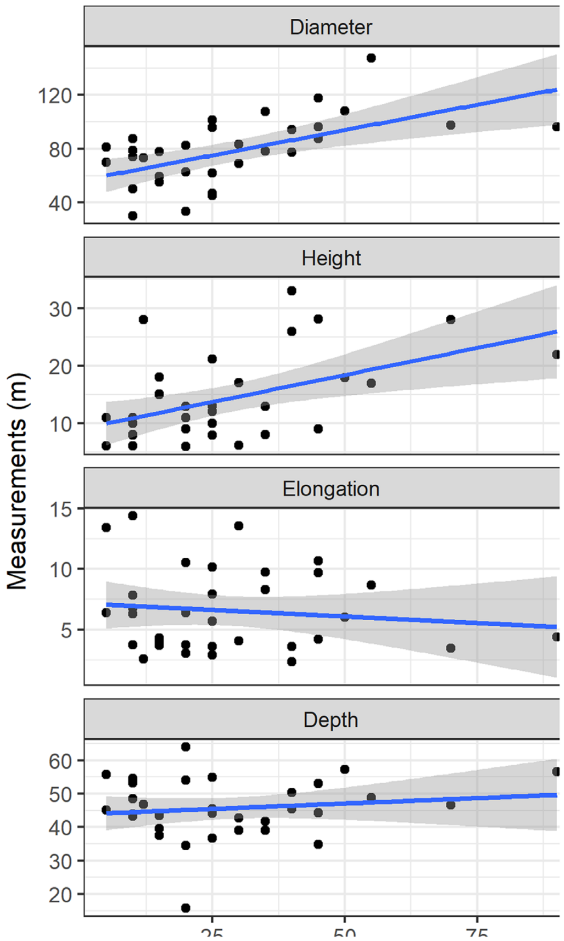

Figure 10. Scatterplot of the typical (distortion-corrected) morphology of tuna aggregations against catch observed around dFADs in this study. All *y*-axes are in meters except the elongation, which is unitless.

Table 3. Linear relationship model parameters between the catch and some of the school morphometric parameters obtained acoustically for the sets analysed.

Response	Explanatory	Intercept	Slope	*R*-squared	*p*-value
Catch	Horizontal diameter	−4.5	0.4	0.3	0.0006
Catch	Height	10.5	1.2	0.2	0.005
Catch	Elongation	33.7	−0.7	0.01	0.5
Catch	Depth	14.4	0.3	0.02	0.4

catches (Figure 10, Table 3). These results are in agreement with those obtained by Peña *et al.* (2021), are in line with other recent efforts to improve quantitative use of multibeam sonars (Vatnehol *et al.*, 2017, 2018; Macaulay and Peña, 2018) and suggest that sonars can be reliable samplers of fish schools, for estimating their size as a preliminary step to estimate their abundance.

Conclusions

- The SN90 multibeam sonar dimension measurements have a higher distortion in athwart-beam than along-beam direction. Along-beam measurements can be reliably read directly from a sonar display. Athwart measurements must be corrected for a reliable interpretation.
- The along-to-athwart fractions, within the ranges of distance to shoals that occur during purse-seine maneuvers (between 225 and 325 m) were ∼0.6 and ∼0.3 were for the horizontal and vertical swath, respectively.
- At longer distances, however, the corrections grow, because of both geometrical spreading and overlapping.
- An analytical correction equation is proposed to correct the beam overlap-based Athwart distortion. The correction is based on determining the percentage of overlap, a simple parameter proposed to characterize multibeam sonars.
- A methodology is also proposed to experimentally measure the percentage of overlap of any type of multibeam sonar. This methodology was proved to be more reliable for sloped-horizontal than for vertical sonar swaths.
- Once the athwart distortion is corrected for, SN90 multibeam sonars appear to be able to provide unbiased, reliable measurements of tuna (and predictably other species) school sizes, and could be used to improve the management of tropical tuna species by defining new indices of abundance independent from the catch, allowing more selective fishing, and a better understanding of tuna behaviour around dFADs.

Acknowledgements

This study has been funded by the Basque Government (EUSKO JAURLARITZA—GOBIERNO VASCO, Ekonomiaren Garapen eta Azpiegitura Saila—Department of Economic Development and Infrastructures, Nekazaritza, Arrantza eta Eli. Politika sail—Vice. de Agricultura, Pesca y Politica Alimentaria, Dirección de Pesca y Acuicultura); as well as the Spanish Government (Administración del Estado, Ministerio de Agricultura, Pesca y Alimentación, DG del Medio Natural y Política Forestal Ministerio de Medio Ambiente y Medio Rural y Marino, Ministerio de Agricultura y Pesca, Alimentación y Medio Ambiente, Secretaría General de Pesca), under the Next Generation Funds Program. In addition, this project received funding under award NA19NMF4720214 from the 2019 Bycatch Reduction Engineering Program NOAA from National Marine Fisheries Service (NMFS) and National Oceanic and Atmospheric Administration (NOAA); and had the additional support of the International Seafood Sustainability Foundation (ISSF). We would like to thank the following organizations and people for their invaluable help in carrying out this work: ALBACORA S.A., for their consent and help to carry out the research and accommodation on board the vessel PACIFIC STAR; the skipper Francisco Javier Alarcia Curiel, captain Gorka Dima del Campo, chief engineer Francisco Javier Baz Rodriguez, and the entire crew of the B/P PACIFIC STAR for their commitment and collaboration with the research activities carried out. We also thank Rolph Korneliussen and the acoustic science team in Institute of Marine Research in Bergen, Norway, for his assistance in the use of the LSSS and PROFOS software.

Supplementary data

Supplementary material is available at the *ICESJMS* online version of the manuscript.

Conflict of Interest

The authors declare that the research was conducted in the absence of any commercial or financial relationships that could be construed as a potential conflict of interest.

Author's contributions

GB, UM, HP, GM, and JU conceived the ideas for the study. GB, UM, and HP designed the methodology. UM acquired the data. GB, UM, and JU analysed the data with close supervision by HP. GB developed the analytical equations. GB led the writing of the manuscript, while HP and GM contributed significantly. All authors gave final approval for publication.

Data availability

The data underlying this article will be shared on reasonable request to the corresponding author.

References

Boyra, G., Moreno, G., Sobradillo, B., Pérez-Arjona, I., Sancristobal, I., and Demer, D. A. 2018. Target strength of skipjack tuna (*Katsuwanus pelamis*) associated with fish aggregating devices (FADs). ICES Journal of Marine Science, 75: 1790–1802.

Boyra, G., Moreno, G., Orue, B., Sobradillo, B., and Sancristobal, I. 2019. In situ target strength of bigeye tuna (*Thunnus obesus*) associated with fish aggregating devices. ICES Journal of Marine Science, 76: 2446–2458.

Castro, J., Santiago, J., and Santana-Ortega, A. 2002. A general theory on fish aggregation to floating objects: an alternative to the meeting point hypothesis. Reviews in Fish Biology and Fisheries, 11: 255–277.

Demer, D. A., Andersen, L. N., Bassett, C., Chu, D., Condiotty, J., Cutter, G. R., Hutton, B. *et al.* 2017. 2016 USA–Norway EK80 workshop report: evaluation of a wideband echosounder for fisheries and marine ecosystem science. ICES Cooperative Research Reports (CRR). ICES. 69pp.

Diner, N. 2001. Correction on school geometry and density : Aquatic Living Resources, 14: 211–222.

Doray, M., Boyra, G., and van der Kooij, J. 2021. ICES survey protocols – manual for acoustic surveys coordinated under the ICES working group on acoustic and egg surveys for small pelagic fish (WGACEGG). ICES Techniques in Marine Environmental Sciences, 64: 100.

Gerlotto, F., Castillo, J., Saavedra, A., Barbieri, M. A., Espejo, M., and Cotel, P. 2004. Three-dimensional structure and avoidance behaviour of anchovy and common sardine schools in central southern Chile. ICES Journal of Marine Science, 61: 1120–1126.

Hewitt, R. P., Brown, J. C., andP. E. 1976. The development and use of sonar mapping for pelagic stock assessment in the California Current Area. United States Fisheries Bulletin, 74: 281–300.

Holmin, A. J., Handegard, N. O., Korneliussen, R., and Tjo/stheim, D. 2011. Simulations of multibeam sonar echos from schooling individual fish. The Journal of the Acoustical Society of America, 129: 2632.

Kongsberg. 2020. Kongsberg Simrad SN90 user manual. 202pp.

Korneliussen, R. J., Heggelund, Y., Eliassen, I. K., Øye, O. K., Knutsen, T., and Dalen, J. 2009. Combining multibeam-sonar and multifrequency-echosounder data: examples of the analysis and imaging of large euphausiid schools. ICES Journal of Marine Science, 66: 991–997.

Korneliussen, R. J., Heggelund, Y., Macaulay, G. J., Patel, D., Johnsen, E., and Eliassen, I. K. 2016. Acoustic identification of marine species using a feature library. Methods in Oceanography, 17: 187–205.

Lopez, J., Moreno, G., Boyra, G., and Dagorn, L. 2016. A model based on data from echosounder buoys to estimate biomass of fish species associated with fish aggregating devices. Fishery Bulletin, 114: 166–178.

Macaulay, G., and Peña, H. 2018. The SONAR-netCDF4 convention for sonar data. Version 1.0. GitHub. 33pp.

Marçalo, A., Breen, M., Tenningen, M., Onandia, I., Arregi, L., and Gonçalves, J. 2019. Mitigating slipping-related mortality from purse seine fisheries for small pelagic fish: case studies from European Atlantic waters: reducing discards in complex, multi-species and multi-jurisdictional fisheries. *In* The European Landing Obligation. Springer International Publishing, New York, NY. 297–318pp.

Medwin, H., and Clay, C. S. 1998. Fundamentals of Acoustical Oceanography. Academic Press, San Diego, CA. 739pp.

Misund, O. A. 1993. Dynamics of moving masses: variability in packing density, shape, and size among herring, sprat, and saithe schools. ICES Journal of Marine Science, 50: 145–160.

Misund, O. A., and Beltestad, A. K. 1996. Target-strength estimates of schooling herring and mackerel using the comparison method. ICES Journal of Marine Science, 53: 281–284.

Moreno, G., Dagorn, L., Capello, M., Lopez, J., Filmalter, J., Forget, F., Sancristobal, I. *et al.* 2016. Fish aggregating devices (FADs) as scientific platforms. Fisheries Research, 178: 122–129.

Moreno, G., Boyra, G., Sancristobal, I., Itano, D., and Restrepo, V. 2019. Towards acoustic discrimination of tropical tuna associated with fish aggregating devices. Plos ONE, 14: 1–24.

Orue, B., Lopez, J., Moreno, G., Santiago, J., Boyra, G., Uranga, J., and Murua, H. 2019. From fisheries to scientific data: a protocol to process information from fishers' echo-sounder buoys. Fisheries Research, 215: 38–43.

Peña, H., Macaulay, G. J., Ona, E., Vatnehol, S., and Holmin, A. J. 2021. Estimating individual fish school biomass using digital omnidirectional sonars, applied to mackerel and herring. ICES Journal of Marine Science, 78: 940–951.

Reid, D. G. 2000. Report on Echo Trace Classification. ICES Cooperative Research Report, 238. 107pp.

Simmonds, E. J., and MacLennan, D. N. 2005. Fisheries Acoustics: Theory and Practice. 2 edn. Blackwell Publishing, Hoboken, NJ. 472pp.

Trygonis, V., Georgakarakos, S., and Simmonds, E. J. 2009. An operational system for automatic school identification on multibeam sonar echoes. ICES Journal of Marine Science, 66: 935–949.

Trygonis, V., and Kapelonis, Z. 2018. Corrections of fish school area and mean volume backscattering strength by simulation of an omnidirectional multi-beam sonar. ICES Journal of Marine Science, 75: 1496–1508.

Uranga, J., Arrizabalaga, H., Boyra, G., Hernandez, M. C., Goñi, N., Arregui, I., Fernandes, J. A. *et al.* 2017. Detecting the presence-absence of bluefin tuna by automated analysis of medium-range sonars on fishing vessels. Plos ONE, 12: 1–18.

Uranga, J., Arrizabalaga, H., Boyra, G., Hernandez, C., and Goñi, N. 2019. Counting and sizing Atlantic bluefin tuna schools using medium range sonars of baitboats in the Bay of Biscay. Continental Shelf Research, 182: 37–45.

Vatnehol, S., Totland, A., and Ona, E. 2015. Two mechanical rigs for field calibration of multi-beam fishery sonars. Methods in Oceanography, 13–14: 1–12.

Vatnehol, S., Peña, H., and Ona, E. 2017. Estimating the volumes of fish schools from observations with multi-beam sonars. ICES Journal of Marine Science, 74: 813–821.

Vatnehol, S., Peña, H., and Handegard, N. O. 2018. A method to automatically detect fish aggregations using horizontally scanning sonar. ICES Journal of Marine Science, 75: 1803–1812.

Handling Editor: David Demer